Finite element simulation and experimental validation of fretting wear

I.R. McColl, J. Ding, S.B. Leen*

School of Mechanical, Material, Manufacturing Engineering and Management

University of Nottingham, UK

Abstract

A finite element-based method is presented for simulating both the fretting wear and the evolution of fretting variables with number of wear cycles in a cylinder-on-flat fretting configuration for application to aeroengine transmission components. The method is based on a modified version of Archard's equation and is implemented within a commercial finite element code. Fretting tests are employed to determine the coefficient of friction and the wear coefficient applicable to the contact configuration and loading conditions. The wear simulation technique is incremental in nature and the total simulation time has been minimised via mesh and increment size optimisation. The predicted wear profiles have been compared with profilometer measurements of fretting test scars.

Keywords: wear, fretting wear, finite element, contact, friction, simulation, Super CMV

*Corresponding author. Tel.: 0044-0115-9513812; fax: 0044-0115-9513800; email address: s.leen@nottingham.ac.uk. Mail address: School of Mechanical, Material, Manufacturing Engineering and Management, University of Nottingham, NG7 2RD, UK

Notation

a	contact half-width
A	apparent contact area
b	width of the flat specimen
c_j	minimum gap between the worn surfaces due to the wear of the j^{th} increment
E	Young's modulus
h	total wear depth
$\Delta h_{i,j}$	wear depth increment at node i for j^{th} wear increment
Δh_{crit}	critical wear depth increment
h_m	average wear scar depth
h_{max}	maximum wear scar depth
H	hardness of the material
k	dimensional Archard wear coefficient
K	non-dimensional Archard wear coefficient
k_l	local wear coefficient
N_t	total number of wear cycles
ΔN	increment in number of simulation wear cycles
ΔN_{crit}	critical value of ΔN for stability
p_0	maximum Hertzian contact pressure

$p_{i,j}$	contact pressure at node i for j^{th} wear increment
$p(x)$	contact pressure as a function of x-position
P	applied normal load
R	radius of contacting surface
$s_{i,j}$	contact slip during a quarter cycle at node i for j^{th} wear increment
S	total (accumulated) slip distance
t	time
$T(t)$	frictional force at time t
T_{max}	maximum frictional force during one fretting cycle
V	total wear volume
W	wear scar width
x,y	rectangular co-ordinates
$y_{i,j}$	y coordinate of node i at beginning of j^{th} wear increment
δ^*	applied stroke half-amplitude
μ	coefficient of friction
σ_x, σ_y	normal stresses on planes perpendicular to the x, y axes
ν,	Poisson's ratio
ω	maximum penetration depth used in ABAQUS contact algorithm

Introduction

Fretting wear is a surface degradation process in which removal of material is induced by small-amplitude oscillatory movement between

contacting components, such as flexible couplings and splines, jointed structures and so on. Analysis of the mechanisms of this type of surface damage has been extensively developed [1-4]. The main parameters affecting fretting wear are reported to be normal load, slip amplitude, frequency, contact geometry, surface roughness and material properties. The "fretting map" approach, established by Vingsbo et al. [5] and Vincent et al. [6], has shown that fretting damage evolution depends strongly on the fretting regime. Debris is also a critical factor influencing fretting wear. It was reported that, once debris accumulates on the contact surfaces and forms a compact oxide layer, the wear rate is significantly reduced [4]. In recent years, Godet et al. developed the theories of third-body tribology [7] and velocity accommodation mechanisms [8] to explain the role of wear debris in specific fretting conditions.

Compared with the development of qualitative understanding, quantitative assessment of fretting wear is less well advanced. One of the difficulties is the absence of a "universal" and well-formulated wear model [9]. In addition, it is not clear how to incorporate the effect of wear debris into such a quantitative model. For some situations, where wear debris is easily eliminated from the contact area and metal-to-metal contact is maintained, the influence of the debris can be reasonably neglected. In such cases, fretting wear can therefore be regarded as a purely contact-based wear problem. Analytical techniques for such problems were developed by Korovchinsky [10], Galin [11], Galin and Goryacheva [12], amongst others.

Goryacheva et al. [13] proposed an analytical method to simulate fretting wear under partial slip conditions for two-dimensional, initially Hertzian configurations. In this model, Archard's equation is applied locally to evaluate wear and the gap variation within the slip zones during one cycle. A stepwise procedure is then employed to calculate the evolution of the contact characteristics as a function of increasing numbers of wear cycles. Johansson [14] presented a finite element solution that incorporates a local implementation of Archard's equation to evaluate the change of contact geometry and the associated changes in contact pressure. More recently, Oqvist [15] presented a study on the numerical simulation of mild wear between a cylindrical steel roller and a steel plate in a reciprocating contact configuration. Measurements of worn topographies were also obtained and good correlation between the numerically predicted and experimentally measured worn profiles was established over about 1 million cycles. However, little detail on the numerical approach employed, which was based on earlier work by Podra and Andersson [16], was provided by Oqvist.

In this paper, the development and initial validation of a detailed finite element model, which simulates the frictional contact behaviour of a cylinder-on-flat fretting test configuration, is first described. This finite element model is then employed, via geometrical updating, as the frictional contact solver for an incremental fretting wear simulation tool, which predicts the change of geometries (i.e. for both contact surfaces) and the associated evolution of salient fretting variables, that is, relative slip, contact pressure and sub-surface

stresses, during the wear process. The geometrical updating is based on nodal wear depths computed using a modified version of Archard's equation for sliding wear. Important aspects, such as mesh refinement and optimisation of numbers of wear cycles per increment, for minimisation of the total simulation time, are discussed. Experimental testing of the same fretting configuration using a high-strength aerospace steel is also described. The tests employed a nitrided against non-nitrided contact pair, as commonly used in aeroengine splines, under a range of normal loads, giving rise to different fretting wear trends and thereby facilitating experimental validation and interpretation of the simulation results. This work forms the basis of a more general fretting wear simulation tool for complex three-dimensional geometries, with future incorporation of the effects of fretting debris.

2. Experimental procedure

2.1 Material and specimens

The material used in this study was a high-strength alloy steel named Super CMV, which is employed in gas turbine aeroengine transmission components, such as spline couplings; the composition is shown in Table 1.

The test materials were initially machined to specimen blanks slightly in excess of the required dimension of specimens. Those blanks were heated to 940°C for 45 minutes followed by oil quenching. The surface hardness after quenching was around 700HV0.3. The blanks were then tempered at 570°C for 2 hours and 15 minutes, followed by air-cooling. The final hardness was

480-510HV0.3. The heat-treated blanks were finally machined and ground to obtain the desired shape and size for the crossed cylinder-on-flat fretting test arrangement. Afterwards, the flat specimens were nitrided to enhance the surface hardness to about 800HV0.3, following a practice commonly employed for improved wear performance of gas turbine aeroengine spline couplings.

Figure 1a shows the topographical features of the flat specimen after nitriding. Figure 1b is a cross section view of the nitrided specimen. A 'white layer' with a thickness of about 6-7μm can be seen. This layer has been identified as a heterogeneous mixture of γ'-(Fe_4N) and ε-$(Fe_{2\text{-}3}N)$ phases and contains high internal stresses in the transitional regions between the various lattice structures [17]. The internal stresses make the white layer very brittle so that it can easily spall off during fretting wear, especially under high contact loads. The cylindrical specimens were not nitrided.

2.2 Fretting tests

The fretting tests were conducted using a crossed cylinder-on-flat arrangement as illustrated in Figure 2. The diameter of the cylindrical specimens was 12 mm. The flat specimen was rigidly attached to the bed of the machine; the cylindrical specimen was driven by an electromagnetic vibrator. A linear variable displacement transducer mounted across the specimen holders monitored the applied stroke. The stroke was automatically maintained constant throughout the tests, except for the initial stages when manual adjustment was required. The normal load was applied by dead weight

via a lever. During the tests, the tangential friction force was measured by strain gauges attached to the drive arm. More detail on this fretting rig can be found in [18]. The fretting conditions used in this study are summarised in Table 2.

3 Experimental results

3.1 Coefficient of friction

The coefficient of friction (*COF*), μ, is defined as the ratio of the measured maximum friction force amplitude during one cycle, T_{max}, and the applied normal load P, as follows:

$$\mu = \frac{T_{max}}{P} \tag{1}$$

Figure 3 shows the change of COF with the number of wear cycles under different (normal) contact loads. *COF* increases rapidly in the initial stages of testing, especially under 185 and 500N normal loads. When the number of wear cycles exceeds 2000 cycles, *COF* tends towards a stable value. The initially low *COF* can be attributed to the presence of surface oxide films. Once the oxide films are eliminated, metal-metal and/or metal-wear particle interactions start, promoting a strong increase in *COF*. From Figure 3, it is also found that the stable *COF* is reduced with an increase in normal load. Specifically, the *COF* for 185N normal load is the highest at ≈ 0.8. It decreases to 0.75 and then 0.6 when the normal load is increased to 500 and 1670N, respectively. This trend is consistent with previous observations [19],

and has been attributed to the interfacial shear stress being a function of a constant value τ_0 and a product of mean contact pressure p and the interfacial shear stress coefficient γ [20].

3.2 Wear results

It is well known that the limited wear damage under fretting is difficult to measure. In the current study, the wear extent was evaluated from two-dimensional surface profiles traced using a SURFCOM 200 scanning stylus profilometer. In general, a horizontal magnification of ×85 and a vertical magnification of either ×1000 or ×2000 were employed. The unworn surfaces were used as the reference surface. Compact oxide debris was removed from the wear scar surfaces before profiling using 3% HCl solution. There were two objectives to the profilometry measurements. First, to obtain appropriate estimates of the wear coefficient for input to the wear simulation tool, and second, to obtain worn profiles for validation of the numerically predicted profiles, as described in Sections 5 and 6. This section describes how the wear coefficient was determined and presents a summary of the worn profiles for subsequent comparison against the numerical predictions. The simulation tool of Section 5 requires a wear coefficient, k_l, expressed as the wear per unit local slip per unit local contact pressure. From experimental results it is only possible to directly measure the wear coefficient per unit displacement per unit normal load. The latter is the Archard wear coefficient, which is defined by:

$$k = \frac{V}{SP} \tag{2}$$

where, for fretting wear, S, the total accumulated displacement, is equal to $4N_t\delta^*$, where δ^* is the displacement amplitude (i.e. half-stroke), V is the total wear volume and N_t is total number of wear cycles.

Direct calculation of the desired wear coefficient requires knowledge of the local contact slips and local contact pressures. As these are not readily measurable a modified form of equation (2) was used to determine an averaged wear coefficient from the measured wear profiles using:

$$k = \frac{Wbh_m}{4\delta^* N_t P} \tag{3}$$

where W is the wear scar width, b is the width of the flat specimen and h_m is the average wear scar depth, with respect to x-coordinate. It should be appreciated that this wear coefficient is averaged across a range of contact pressures and slips, as well as across an appreciable number of wear cycles, and is thus not ideal. However, its use is necessary until the wear simulation tool is sufficiently developed to enable the local contact pressures and slips to be calculated from the measured wear profiles.

The two-dimensional wear profiles in the fretting (x) direction were roughly similar across the width of the flat specimen and along the complementary length of the cylindrical specimen, so that, for present purposes, a representative measured profile is employed to obtain the necessary data for wear coefficient calculation. Figure 2 shows that the width of the flat specimen, b, is 10mm. The two-dimensional surface profiles for the

flat and cylindrical specimens are shown in Figure 4, corresponding to the case of 185N normal load. The mean wear depth of the measured scar, h_m, is evaluated by averaging a series of ten discrete values of wear depth, h_i, at different positions along the scar, from the profilometer trace. A maximum wear depth for the flat specimen, h_{max}, is also obtained from the measured wear scar profile.

The wear coefficients for the cases of Table 2 are presented in Figure 5. The results are seen to vary with normal load. With respect to the flat specimen, the wear coefficient increases with normal load increase from 185N to 500N, and decreases when the normal load continues to increase to 1670N. However, the coefficients of the cylindrical specimens remain almost constant with respect to normal load variation. The effect of normal load on the wear coefficient is attributed to (a) the presence of the white layer on the surface of the flat specimens, which is brittle and fragments easily under high normal loads thus contributing to the measured wear rates, and (b) the different tribological behaviour of debris under different contact loads. More detailed interpretations on this matter will be presented in future work.

4. FE model for fretting contact

4.1 Development of FE model

The basis for the fretting wear prediction tool described in the next section is a detailed, two-dimensional, finite element model of the fretting test geometry. The general purpose, non-linear code, ABAQUS [21], was employed for the FE modelling, to facilitate generalization of the present approach to more complex applications. The finite element model is shown in Figure 6, where the radius of the cylinder is the same as the cylindrical specimen in the fretting tests. Two-dimensional, four-node, plane strain (linear) elements are employed throughout. The mesh (element size) in the contact area is very fine (about 10μm) to capture the complicated variation of surface and sub-surface stresses and relative slip. The sharp transition from coarse mesh, remote from the contact region, to fine mesh, in the contact region, is achieved via multi-point constraints (MPCs). This is necessary to achieve the correct balance of detailed contact region mesh refinement, for modelling microscopic wear depth increments and for accurate prediction of the salient fretting variables, and minimal CPU time for the total wear simulation, e.g. 18,000 cycles. As discussed below, a typical incremental number of wear cycles is about 30, each increment requiring one combined normal and tangential loading analysis, so that a total number of 18000 wear cycles requires about six hundred individual FE analyses. Optimisation of the mesh has led to reductions in total wear simulation time from about six days to less than one day. The contact surface interaction is defined via the contact

pair approach in ABAQUS, which uses the master-slave algorithm to enforce the contact constraints. The nodes on the slave surface are permitted to penetrate the master surface by a user-controlled maximum penetration depth, ω. The cylindrical surface is chosen as the slave contact surface and a ω value of approximately 5μm is found to be satisfactory. The basic Coulomb friction model with isotropic friction is employed. The frictional contact conditions are introduced via the Lagrange multiplier approach, rather than the more approximate penalty method, in order to enforce exact sticking (zero slip) constraints between the bodies when the equivalent shear stress is less than the critical shear stress. During the loading scheme, linear constraint equations are employed to ensure uniform displacement of the nodes on the top surface of the cylinder. The bottom of the flat substrate is restrained from movement in the x and y directions. The elastic modulus and Poisson's ratio of both the cylinder and flat are taken as 200GPa and 0.3, respectively.

In order to validate the accuracy of the unworn model, comparisons are made with the well-known analytical solutions for the Hertzian stress distributions [22]. The contact pressure distribution is given:

$$p(x) = p_o \sqrt{1 - \frac{x^2}{a^2}} \tag{4}$$

The half-width of the contact area, a, and the maximum contact pressure, p_0, are, respectively, given by:

$$a = \left(\frac{4PR}{\pi E^*} \right)^{\frac{1}{2}} \tag{5}$$

$$p_o = \left(\frac{PE^*}{\pi R} \right)^{\frac{1}{2}} \tag{6}$$

where P is the applied normal load and E^* is the composite modulus of the two contacting bodies. For plane strain conditions the latter is given by:

$$E^* = \left(\frac{1-(\nu^f)^2}{E^f} + \frac{1-(\nu^c)^2}{E^c} \right)^{-1} \tag{7}$$

where E^f, E^c are the elastic moduli of the flat and cylindrical bodies, respectively, and ν^c, ν^f are the corresponding Poisson's ratios. R is the relative curvature given by:

$$R = \left(\frac{1}{R^f} + \frac{1}{R^c} \right)^{-1} \tag{8}$$

wher R^f and R^c are the radii of the contacting surfaces. Figure 7a shows a comparison of $p(x)$ from Equation (4) and the corresponding FE-predicted distribution using the mesh of Figure 6. Elasticity theory [22] allows the sub-surface x and y direction normal stresses along the y-axis (principal stresses) to be derived:

$$\sigma_x = -\frac{p_o}{a} \left\{ \left(a^2 + 2y^2\right)\left(a^2 + y^2\right)^{-1/2} - 2y \right\} \tag{9}$$

$$\sigma_y = -\frac{p_o}{a} \left(a^2 + y^2\right)^{-1/2} \tag{10}$$

Figure 7b shows a comparison between the latter stress distributions and the corresponding FE predictions. The finite element model is seen to give excellent agreement with the analytical solution for all three variables, thus indicating satisfactory mesh refinement.

4.2 Fretting contact under combined normal and tangential loading

In the fretting wear tests, the crossed cylinder-against-flat specimens of Figure 2 are subjected to fixed normal contact loading with superimposed cyclic tangential displacement, for the test data shown in Table 2. This loading cycle must therefore be implemented within the FE model in order to permit wear calculations. Referring to Figure 6, the loading history for the FE model is as follows: a normal load is applied to Point *A* in the *y* direction, in one analysis step, and then a periodic x-displacement of amplitude δ^* is imposed at Point *B*, in two subsequent analysis steps, introducing an oscillatory tangential friction force, *T(t)*, on the contacting surfaces.

The contact pressure distribution under fretting conditions is consistent with the Hertzian solution, since the distribution is independent of the tangential load or displacement when the contacting bodies have the same Young's modulus [22]. Note that this is not the case in the presence of wear as described in Section 6. It is well known that under fretting conditions the actual relative slip between contacting components differs more significantly from the applied tangential stroke or displacement than under, for example, sliding conditions. It is the relative slip that is employed for fretting wear prediction, rather than the applied stroke, even though applied stroke is conventionally employed for wear coefficient evaluation from test data. This is due to the direct availability of the applied stroke data and the difficulty of estimating relative slip for a given test configuration. It is not generally possible to obtain the slip distribution analytically for displacement-controlled

conditions, although analytical solutions are available for some simplified configurations under load control [22]. In any case, the objective of the present work is to develop a general tool for application to complex geometries such as spline teeth. Figure 8 shows the FE-predicted relationship between contact slip, for an applied (at point *A*) bulk displacement of 2.5μm, under a range of normal loads. The results demonstrate the evolution from the gross slip regime under low normal loads, e.g. 600N to 1000N, to the partial slip regime under higher normal loads, e.g. 1200N to 1600N; in both cases, it is clear that relative slip at the contact interface is significantly less than the applied displacement. The relative slip varies with horizontal position along the contact interface, being lower in magnitude at the centre than at the edges of contact. This spatial variation of slip gives rise to a corresponding variation of local wear depth with horizontal position, as shown below.

5 Wear simulation method

5.1. Wear model

Following the hypothesis of Stowers and Rabinowicz [23] and as implemented by Johansson [14], it is assumed here that fretting wear can be evaluated by applying Archard's equation to local contact conditions along a differential width of the contact interface. Archard's equation for sliding wear is normally expressed as [24]:

$$\frac{V}{S} = K\frac{P}{H} \tag{11}$$

where K is the dimensionless wear coefficient and H is the hardness (MPa) of the material. P, S and V have been defined in Section 3. In order to simulate the evolution of the contact surface profiles with wear cycles, it is necessary to determine the wear depth locally as a function of horizontal contact position, x, i.e. at each contact node of the finite element model. Therefore, for an infinitesimally small apparent contact area, dA, the increment of wear depth, dh, associated with an increment of sliding distance, dS, is determined. This can be obtained by applying Equation (11) locally to the area dA and for the increment of sliding distance, dS:

$$\frac{dV}{dS} = K\frac{dP}{H} \tag{12}$$

Then, dividing both sides by dA, the following equation is obtained:

$$\frac{dV}{dAdS} = K\frac{dP}{HdA} \tag{13}$$

The dP/dA term is the local contact pressure, $p(x)$, while dV/dA is simply equal to the required increment of local wear depth, dh, noting that h is a function of both horizontal position x and the total local slip distance, S. The following equation is thus obtained for the prediction of the increment of local wear depth:

$$\frac{dh}{dS} = k_l\, p(x) \tag{14}$$

where the quantity K/H is replaced here by k_l, the local wear coefficient. Unfortunately, the authors are not aware of any existing method for estimating k_l. Consequently, the best available alternative is to measure an average value across the complete contact width, as described in Section 3. Thus, in the

present study it is assumed that $k_l \approx k$. The implication of Equation (14) is that the incremental wear depth at a given point on the contact is proportional to the local wear coefficient, the local contact pressure and the local increment of slip distance. In the numerical prediction of fretting wear described below, which may involve either gross slip or partial slip situations, S is assumed to be the total local slip distance between the contacting surfaces. Note again that k, and thus k_l, is obtained using the applied test stroke, which will naturally give an underestimate of the wear volume, since the local contact interface slip is always less than the applied bulk displacement. The degree of underestimation can be expected to decrease with decreasing normal load for a given applied stroke, due to the diminishing difference between applied stroke and contact slip.

5.2 Wear modelling procedure

An automated, incremental, wear simulation tool has been developed based on the wear prediction equation of the above section. This section describes this development for the cylinder-on-flat test arrangement. An important aspect of this work is the use of the ABAQUS commercial finite element code; its general capabilities facilitate extension to other contact geometries, such as flat-on-flat or spline tooth flanks. Figure 9 shows a flowchart of the numerical procedure that forms the basis of the simulation tool. Once the finite element model of the initial, unworn geometry has been generated, the program can be run for any specified number of wear cycles to predict the corresponding worn surface profiles and the evolution of surface

and sub-surface contact variables. The simulation tool consists of an interaction between a special-purpose Fortran program and ABAQUS, whereby the FE model is incrementally updated, as described below, according to the calculated wear depths, based on the local contact pressure and local slip results of the FE analyses.

The initial parameters required for the wear simulation include contact geometry, material properties, normal load, applied stroke and coefficient of friction, all of which are defined within the FE model, along with the governing parameters for wear modelling, namely wear coefficient k_l, the total number of wear cycles N_t and the increment in number of wear cycles per step, ΔN.

The total number of wear cycles, N_t, is discretised into n wear increments and the increment of wear depth, Δh, at each contact node on each surface is then calculated incrementally, for the specified value of ΔN. The choice of a suitable value for ΔN is important for both the stability of the simulation and the resulting computational time, as further discussed in Section 7.

Specifically, for the j^{th} wear increment, at a given node i on either contact surface, the contact pressure, $p_{i,j}$, and slip per cycle, $4s_{i,j}$, are determined using the FE model of Section 4. It is assumed that $p_{i,j}$ and $s_{i,j}$ are constant within a given increment. The increments of wear depth for the flat and cylindrical contact surfaces at node i in the j^{th} increment are then given by

$$\Delta h_{i,j}^{f} = k_l^{f} \times 4s_{i,j} \times \Delta N \times p_{i,j} \tag{15}$$

$$\Delta h_{i,j}^{c} = k_l^{c} \times 4s_{i,j} \times \Delta N \times p_{i,j} \tag{16}$$

where the superscripts *f* and *c* represent the flat and cylindrical surfaces, respectively. Hence, the updated vertical coordinate, $y_{i,j+1}^{f}$, of node *i* at the start of the $j+1^{\text{th}}$ wear increment for the flat surface is given by:

$$y_{i,j+1}^{f} = y_{i,j}^{f} - \Delta h_{i,j}^{f} \tag{17}$$

and the corresponding updated vertical coordinate for the cylindrical surface is given by:

$$y_{i,j+1}^{c} = y_{i,j}^{c} + \Delta h_{i,j}^{c} - c_j \tag{18}$$

The c_j term is the amount by which the FE model of the cylindrical specimen needs to be moved down vertically, i.e. a rigid body movement, to ensure that the contact surfaces are initially in contact at the beginning of the new wear increment. This term is calculated as follows:

$$c_j = \min((y_{i,j}^{c} + \Delta h_{i,j}^{c}) - (y_{i,j}^{f} - \Delta h_{i,j}^{f})) \tag{19}$$

It represents the minimum gap between the worn surfaces due to the wear of the j^{th} increment. Repetition of these calculations for each increment of the total number of wear cycles then achieves the required wear simulation.

One of the most important challenges for the general application of the above method to complex three-dimensional components, such as aeroengine spline couplings, e.g. see [25], where fretting wear assessment is critical to component design optimisation, is the minimisation of the wear simulation times. This is achieved here via a number of different aspects, including mesh

optimisation (see above) and wear increment optimisation (see below). Assessment of the slip distributions during the different stages of the tangential force-displacement cycle has established that the total slip distance for the complete cycle can be satisfactorily estimated from the slip distance, $s_{i,j}$, corresponding to the application of the positive tangential displacement only. Although initial development work was based on slip estimates obtained from incremental simulation of both the positive and negative tangential displacements, the use of $s_{i,j}$ gives a significant saving of 67% on simulation time. This saving is simply due to the observation that it is not necessary to simulate the negative tangential displacement increment to get accurate contact slip estimates for the complete cycle, which in turn results from the near geometrical symmetry of the connection, even in the worn condition.

6. Results

6.1 Predicted wear profiles

The latter approach has been applied for the loading conditions of Table 2. The coefficient of friction and the wear coefficient for each load are given in Section 3 and these values are employed in the respective wear simulations. Figure 10 shows the FE-predicted evolution of the contact surface profiles with increasing fretting wear cycles, for the case of 185N normal load. It is found that as fretting wear proceeds, a wear scar develops in the flat surface while the shape of the round surface is also modified. The contact tends towards conforming, with similar radii on both surfaces.

The numerically predicted worn surface profiles of the flat specimens after 18,000 cycles have been compared with experimental results for all three cases and are presented in Figure 11. The predicted values of scar width and maximum wear depth, together with corresponding experimental results, are presented in Table 3. For the low normal load case of 185N, the predicted and measured results are seen to correlate closely. For the 500N and 1670N cases, the wear scar widths are seen to be over-predicted, by 34% and 16%, respectively, while the maximum wear depths are under-predicted, by 44% and 25%, respectively.

Figure 12 shows a comparison between the wear volumes predicted using: (i) the current wear simulation tool, which employs local contact slip, and (ii) Archard's equation, directly, which uses the applied stroke. The wear volume is plotted against the number of fretting cycles for the three different normal loads. For the 185N load, the Archard equation approach gives very similar results to the wear simulation approach, whereas under the higher loads the disparity is seen to increase with increasing load. For the 1670N case, the difference is about 15%. Note that the Archard wear coefficient is calculated in terms of the worn surface profile at 18,000 wear cycles. Thus, it can be concluded that the local contact slip-based approach gives rather good wear volume prediction for low normal loads but underestimates the wear volumes for high normal loads. This is further discussed below.

6.2 Evolution of contact variables

Figure 13 shows the FE predicted evolution of the half contact width with increasing wear cycles, for the three load cases of Table 2. The predicted width for the unworn geometry is consistent with the Hertzian solution. However, as fretting wear proceeds, the width is obviously modified. There is a rapid increase in contact width over the first 2000 cycles, followed by a gradual reduction in the rate of increase. For subsequent cycles, the contact width continues to increase but at a slower rate.

The contact pressure distribution evolves concomitantly with the changes of contact width. Figure 14 shows the FE predicted evolution of the contact pressure distribution with increasing wear cycles, for the 185N normal load; these distributions correspond to the zero tangential displacement position in the fretting cycle. The peak pressure continuously decreases as the distribution along the contact width finally tends towards uniform. The variation of peak pressure for all three cases is demonstrated in Figure 15. There is a dramatic reduction in peak pressure during the first thousand cycles, followed by a significantly more gradual reduction over the subsequent 17,000 cycles. After 18,000 cycles, the peak pressures for all three cases are predicted to have reduced to less than 30% of their initial values.

Figure 16b shows the variation of predicted contact pressure distribution for the set of discrete displacements, δ_A, δ_B, δ_C, δ_D and δ_E, as shown in Figure 16a, during the applied tangential displacement cycle of the 18000^{th} wear cycle. It is clear that there is a significant variation of contact pressure at

any given position along the contact width during this cycle. Initial development work on the present wear simulation approach was based on the use of such instantaneous local pressures and the corresponding local slip values for the wear depth calculations. Comparison against wear simulation results based on the use of a 'representative' local contact pressure and corresponding local slip value, where the 'representative' value was taken as the zero tangential displacement value, established that the results agreed to within 5% for the 18,000 wear cycle case. The use of this 'representative' pressure improves the computational efficiency significantly, reducing the simulation time by approximately 60%. Consequently, the approach of Section 5 is based on the use of the 'representative' contact pressure.

Figure 17 shows the evolution of contact slip, corresponding to the positive tangential displacement point of the fretting cycle (point δ_B of Figure 16a), from the initial unworn case to the worn case, after 18,000 fretting cycles. Note the significant increase in contact width from less than 0.1 mm to about 0.5 mm, as also shown in Figure 13. The slip amplitude, which is predicted to increase by less than 1μm, is however only negligibly affected by the wear damage. This small increase is attributed to the decrease in the contact pressure.

7. Discussion

The advantage of the present approach to fretting wear simulation is that it is based on the use of a commercial FE code and the implementation of the wear simulation tool only requires the development of an additional program

to interact with the FE code, via modification of the model input and processing of the analysis output, to apply the wear depth equations of Section 5, although such a program also needs some built-in intelligence, as described in the paper. The use of a commercial code as the frictional contact solver part of the tool facilitates generalisation to more complex components, as mentioned above, such as three-dimensional contact geometries and couplings, both for industrial application, to predict the wear-limited service life of such components, and also for academic research purposes, to assess, for example, the interaction between fretting wear and crack nucleation in laboratory test configurations. The method is obviously flexible and can be easily transferred into in-house design procedures or other FE codes to assess wear damage and associated changes in stress field. The use of a commercial code also facilitates extension or coupling to simulate related failure phenomena, such as fracture mechanics and crack growth.

One of the most important aspects dealt with throughout the paper is the need for optimisation with respect to computational cost without sacrificing accuracy. Three main techniques related to this described so far are: (i) mesh optimisation, via mesh refinement MPCs and judicious mesh refinement; (ii) the use of symmetry of the tangential force-displacement loop with respect to contact slip, to circumvent simulation of the complete tangential part of each fretting cycle; (iii) the use of ‘representative’ contact pressure and slip values in place of the instantaneous values throughout the tangential cycle.

Another obvious method of reducing the simulation time is to employ a larger value for ΔN. However, it is found that if ΔN exceeds a critical value, ΔN_{crit}, the results become unstable, as shown in Figure 18. In this case, the instability occurs after only 200 cycles, but clearly the consequences are greater if significant computational time has been invested in a greater number of simulated cycles. Similar stability problems were also found in the numerical approaches proposed by Johansson [14] and Oqvist [15]. ΔN_{crit} is found to depend on a number of different input parameters, including normal load, stroke or slip and wear coefficient. For example, for the case of a normal load of 1200N, with a *COF* of 0.6, a stroke of 20μm and a wear coefficient of 1×10^{-8}MPa^{-1}, ΔN_{crit} is approximately equal to 30. However, it is not satisfactory to have to determine ΔN_{crit} iteratively for every load case. Fortunately, the stability problem is more directly interpreted in terms of a maximum allowed wear depth per increment, Δh_{crit}, which is independent of contact load, stroke/slip and wear coefficient and which, if exceeded, is the cause of the instability, via the contact algorithm of the FE code. In a given wear simulation, due to the decreasing contact pressure and the negligible change of contact slip with increasing N, the value of Δh correspondingly decreases continuously. The approach recommended here is to determine Δh_{crit} for one load case and then to determine the stable ΔN for other load case simulations, using trial and error, by comparing the corresponding initial Δh to Δh_{crit}. Figure 19 shows how Δh_{crit} can be determined for one load case. For the chosen load conditions, wear simulations are carried out with a series of

decreasing ΔN values, until instability occurs; it has been found that if instability is to occur, it will do so within the first ten wear increments. A ΔN value is thus obtained for which instability does not occur and the Δh value corresponding to this ΔN is then taken as Δh_{crit}. To ensure against instability for other loading conditions, it is then only necessary to check the initial value of Δh, for a chosen ΔN, against Δh_{crit}. The latter approach can prevent instability but at the cost of increased computation. Oqvist [15] suggested a simple method to balance the simulation time and the stability, by introducing a varying ΔN. This method has also been successfully implemented here.

The comparisons of Figures 11 and 12 and Table 3 show that, as the normal load increases, the FE-based approach underestimates the wear volume, by under-predicting the maximum wear depth and over-predicting the wear scar width. An explanation is that there is less difference between the applied displacement and the calculated contact slip for low normal loads. The fact that contact slip decreases with increasing normal load under the same applied stroke has been schematically demonstrated in Figure 8 and since it was necessary to employ applied stroke for estimation of the wear coefficient (Section 3), the wear damage, based on contact slip, naturally under-estimates wear volume. For the low normal load, this under-estimation is small so that close correlation is obtained. The depth under-predictions for high normal loads are considered to be due to debris effects, caused by the experimentally-observed debris retention on the cylindrical surface, which in turn causes

increased contact pressure and decreased contact slip, and thus increased wear depth, at the centre of the contact scar.

Figure 20 shows a comparison of the measured and predicted loop for the 18000th cycle for the 185N case. Two main differences are observed between the measured and predicted loops. The first is larger inclination of the measured hysteresis loop, reflecting the tangential compliance of the system. The second difference is that the width of the measured loop is smaller than the predicted one. Preliminary calculations have established that applied normal and tangential loads do not give rise to von Mises stresses in excess of the yield stress, so that these differences cannot be attributed to plastic yield. According to Vincent [26], the loop width can be regarded as being approximately equal to an averaged measure of the half-cycle relative slip. This suggests, referring to Figure 20, that the measured slip value is less than the FE-predicted value. This difference can be explained in terms of the displacement accommodation of the fretting system. The velocity accommodation model proposed by Godet [8] shows that in a real (experimental) fretting system, the imposed displacement $2\delta^*$ can be partially accommodated by deformation of the contacting bodies, the third body (debris) and the associated interfaces. This suggests that the FE model employed needs to be enhanced in order to simulate more realistically the fretting conditions. Additional work is required to understand and simulate the mechanical behaviour of the debris and its effect on displacement (velocity) accommodation. This will permit better matching of the predicted and

measured T-δ loops and thus also quantitative identification of the effect of debris on fretting wear damage.

Ultimately, following this future work on incorporation of debris effects, it is anticipated that comparisons between simulation results and measured results will permit estimation of the local wear coefficient, k_l. The availability of such a local wear coefficient, independent of contact geometry and operating conditions, will facilitate general application to new contact geometries and conditions.

The present paper has considered gross slip situations only. The issues of partial slip, where the contact region is divided into the stick and slip zones, has been dealt with in another paper.

8. Conclusions

An incremental method for fretting wear simulation, based on a modified Archard equation, has been applied to a series of gross slip cylinder-on-flat tests on a high-strength, alloy steel for aeroengine applications. The measured and predicted worn surface profiles were found to correlate well for the low normal load case. Under high normal loads, the predicted maximum wear depth was under-estimated and the width of the scar was over-estimated. The differences are attributed to the use of stroke for wear coefficient calculation and the effect of debris, which was not modelled.

During the first 1000 wear cycles, the half contact width increases significantly, by about 100%, while the peak contact pressure decrease dramatically to about 40% of the initial peak Hertzian value; subsequent

changes in these variables are at a slower rate. The contact pressure distribution was shown to evolve to a uniform distribution across the increased contact width. The slip between the contacting bodies was shown to increase slightly with wear, concomitant with the decreasing contact pressure.

A number of techniques for minimisation of the total simulation time were discussed including (i) mesh optimisation, (ii) the informed use of 'representative' contact pressure and slip values, to circumvent simulation of the full fretting cycle, and (iii) optimization of ΔN, the increment in number of simulation wear cycles. A critical incremental wear depth technique for avoidance of stability problems associated with incorrect choice of ΔN has been presented.

Differences between the measured and predicted tangential force-displacement loops, and the associated slip values, have been interpreted in terms of the displacement accommodation effects of debris.

Acknowledgements

The authors would like to thank Rolls-Royce plc for financial assistance, as well as Dr Thomas R Hyde and Mrs Nina Banarjee of Rolls-Royce plc for helpful discussions.

References

1. H.H.Uhlig, "Mechanism of fretting corrision," *Journal of Applied Mechanics*, 21 (1954), pp. 401.

2. P.L Hurricks, “The mechanism of fretting wear – A review,” *Wear*, 15 (1970), pp. 389-409.

3. R.B. Waterhouse, “Fretting wear,” in: ASM handbook, Vol. 18, *Friction, Lubrication, and Wear Technology*, ASM International, pp. 242-256, 1992.

4. D. Aldham, J. Warburton and R.E. Pendlebery, “The unlubricated fretting wear of mild steel in air,” *Wear*, 106 (1985), pp. 177-201.

5. O. Vingsbo and S. Soderberg, “On fretting map,” *Wear*, 26 (1988), pp.131-147.

6. L. Vincent, Y. Berthier and M. Goget, “Testing methods in fretting fatigue: a critical appraisal,” *ASTM STP*, 1159 (1992), pp. 23-32.

7. M. Godet, “The third-body approach: a mechanical view of wear,” *Wear*, 100 (1984), pp. 437-452.

8. Y. Berthier, L.Vincent and M. Godet, “Velocity accommodation in fretting,” *Wear*, 125 (1988), pp. 25-38.

9. H.C. Meng and K.C. Ludema, “Wear models and predictive equations: their form and content,” *Wear*, 181-183 (1995), pp. 443-457.

10. M. V. Korovchinsky, “Local contact of elastic bodies with wear of their surface,” in: *Contact Interaction of Solid bodies and Calculation of Friction Forces and Wear*, Nauka, Moscow, pp. 130-140, 1971.

11. L.A. Galin, “Contact problems of the theory of elasticity in the presence of wear,” *Journal of Applied Math. Mech*., 40 (1976), pp. 981-986.

12. L.A. Galin and I. G. Korovchinsky, “Axisymmetric contact problem of the theory of elasticity in the presence of wear,” *Journal of Applied Math. Mech*., 41 (1977), pp. 826-831.
13. I.G. Korovchinsky, P.T. Rajeev and T.N. Farris, “Wear in partial slip contact,” *Journal of Tribology*, 123 (2001), pp. 848-856.
14. L. Johansson, “Numerical simulation of contact pressure evolution in fretting,” *Journal of Tribology*, 116(1994), pp247-254.
15. Mona Oqvist, “Numerical simulation of mild wear using updated geometry with different step size approaches,” *Wear*, 249 (2001), pp. 6-11.
16. Priit Podra and Soren Andersson, “Simulating sliding wear with finite element method,” *Tribology Internaional*, 32 (1999), pp. 71-81.
17. J. A. Kirk, G.K. Egerton and B. D. Sartwell, *Journal of Lubrication Technology*, 105 (1983), pp. 239.
18. M.M. Hamdy, M.P. Overs and R.B. Waterhouse, “A new high-temperature fretting wear test rig,” *Journal of Physics E Science Instrument*, 14 (1981), pp889.
19. S. Fouvry, “Shakedown analysis and fretting wear response under gross slip condition,” *Wear*, 251(2001), pp 1320-1331.
20. F.P. Bowden and D. Tabor, *Friction and Lubrication of Solids*, Vol. I, Oxford University Press, London, 1964.
21. *ABAQUS User’s and Theory Manuals*, Version 6.1, HKS Inc., Pawtuchet, US, 2001.

22. Johnson, K.L., *Contact mechanics*, Cambridge University Press, Cambridge, 1985.

23. I.F. Stowers and E. Rabinowicz, "The mechanism of fretting wear," *Journal of Lubrication Technology*, 90 (1973), pp. 65-70.

24. J.F. Archard, "Contact and rubbing of flat surfaces," *Journal of Applied Physics*, 24 (1953), pp. 981-988.

25. S. B. Leen, T.R. Hyde, E.J. Williams, A.A. Becker, I.R. McColl, T.H. Hyde and J.W. Taylor, "Development of a representative test specimen for frictional contact in frictional contact in spline joint couplings," *Journal of Strain Analysis*, vol. 35, No 6 (2000), pp. 521-544.

26. S. Fouvry, P. Kapsa and L. Vincent, "Qualification of fretting damage," *Wear*, 200 (1996), pp 186-205.

Table 1 Composition of Super CMV (wt.%).

C	Si	Mn	P	S	Cr	Mo	Ni	V	Fe
0.35-0.43	0.1-0.35	0.4-0.7	<0.007	<0.002	3.0-3.5	0.8-1.10	<0.3	0.15-0.25	Remainder

Table 2 Fretting test conditions

Normal load	185, 500,1670 N
Initial maximum Hertzian stress	336, 550, 1000 MPa
Stroke	50 μm
Frequency	20 Hz
Total number of wear cycles	18,000
Room temperature	14-20°C
Relative humidity	40-50%

Table 3 Comparison of FE prediction and experimental results for wear scar on the flat specimen after 18,000 wear cycle. Stroke is 50μm.

Normal load (N)	Scar width (mm)		Max. wear depth (μm)	
	measured	predicted	measured	predicted
185	0.54	0.52	2.9	3.0
500	0.59	0.79	15.0	8.4
1670	0.75	0.87	15.6	11.7

List of Figures

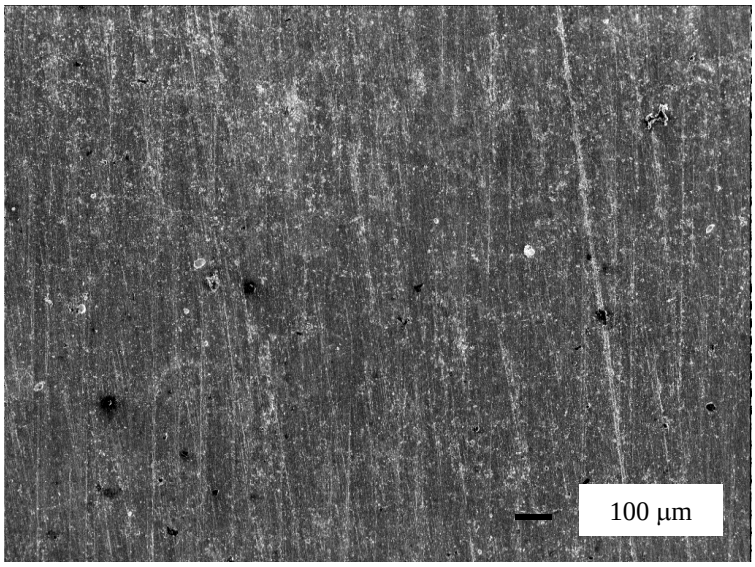

(a)

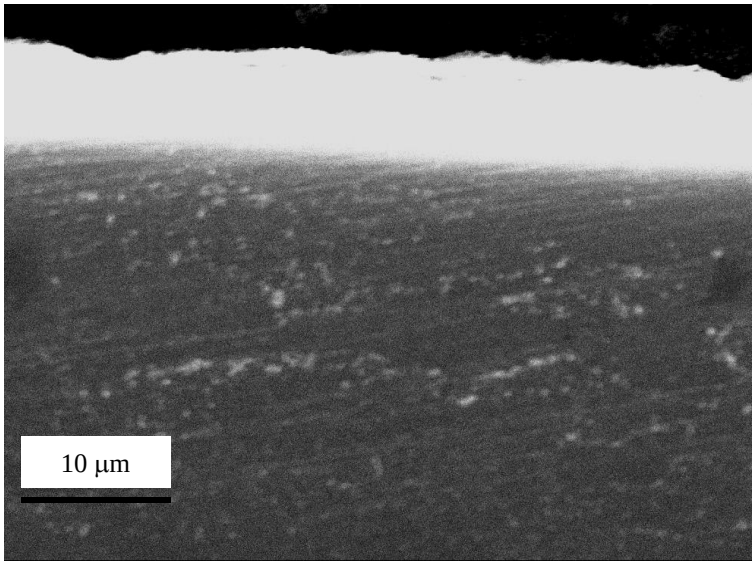

(b)

Figure 1 SEM micrographs of nitrided flat specimen showing (a) plan view and (b) cross-section view, including white layer.

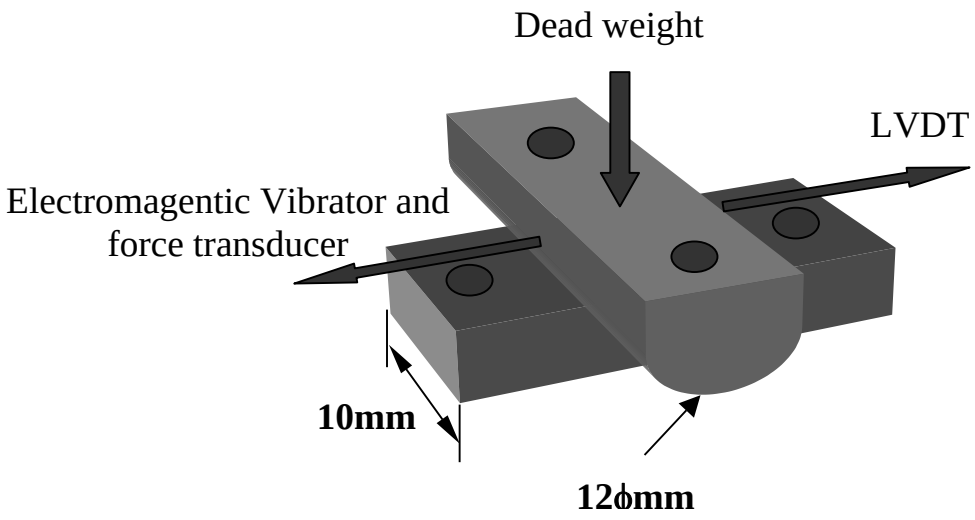

Figure 2 Schematic crossed round-against-flat specimen arrangement

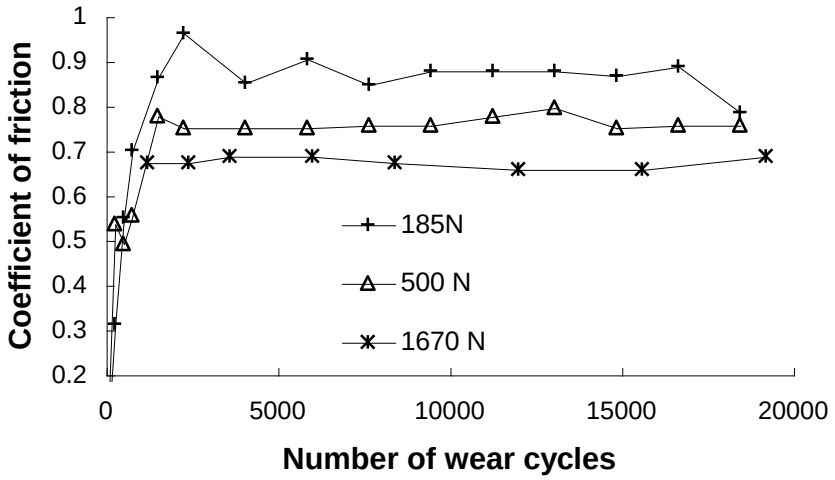

Figure 3 Coefficient of friction versus number of fretting wear cycles. Stroke 50 μm, frequency 20 Hz.

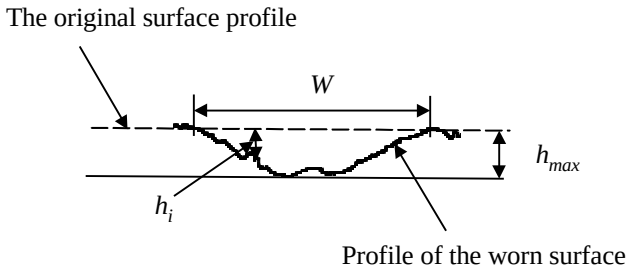

(a) flat specimen

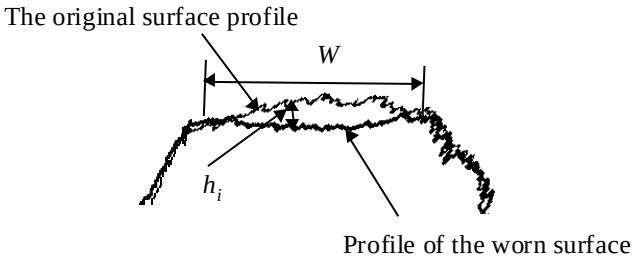

(b) cylindrical specimen

Figure 4 Measured two-dimensional surface profiles of unworn and worn flat and cylindrical specimen for 185 N normal load case.

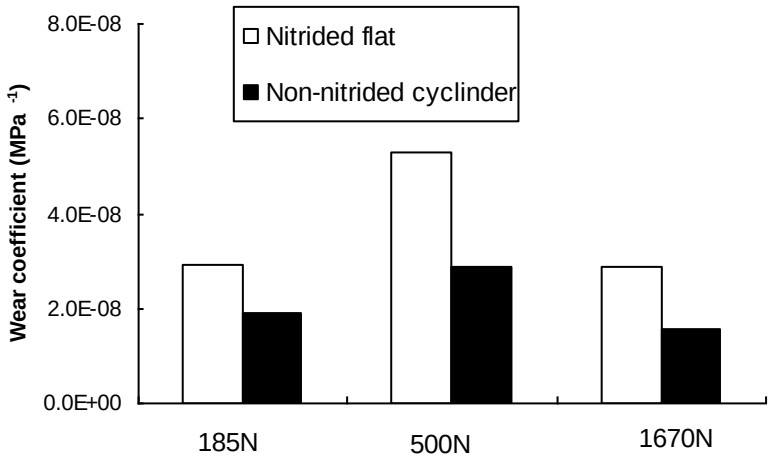

Figure 5 Wear coefficients for the different normal loads.

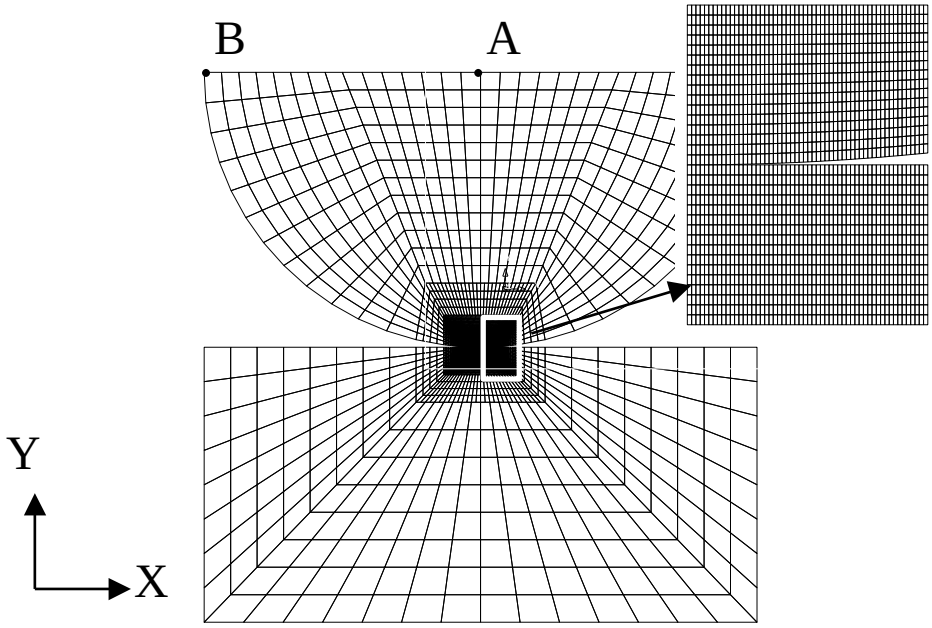

Figure 6. Finite element model for cylinder-on-flat configuration.

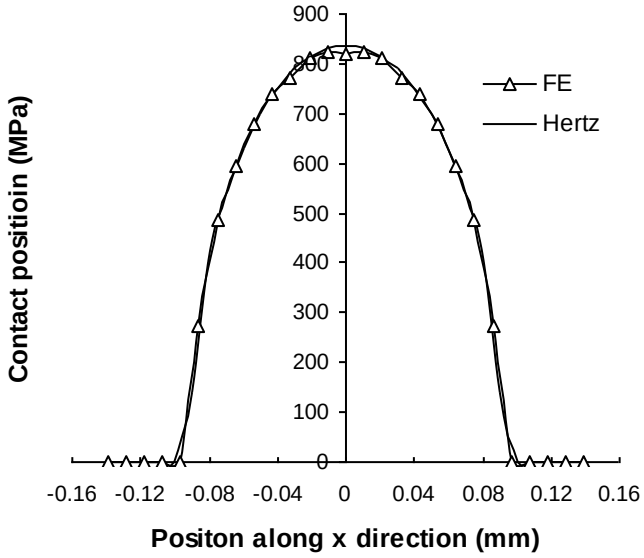

(a)

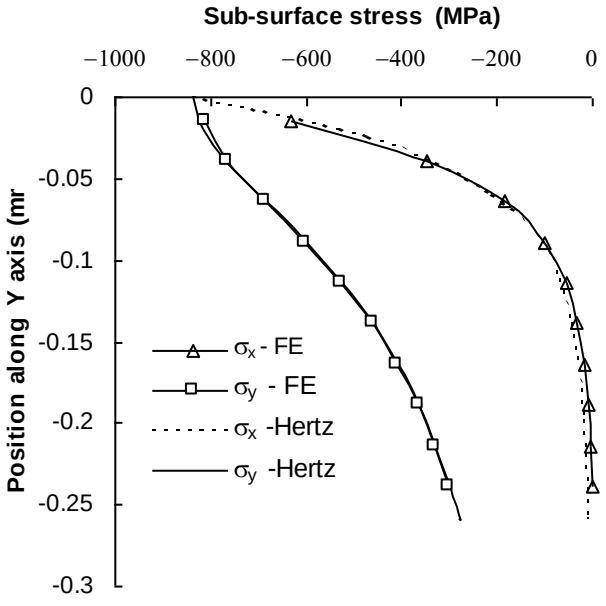

(b)

Figure 7 Comparison of Hertzian problem from FE prediction and analytical solution for (a) distribution of contact pressure and (b) subsurface stress along Y axis under a normal load of 1200 N.

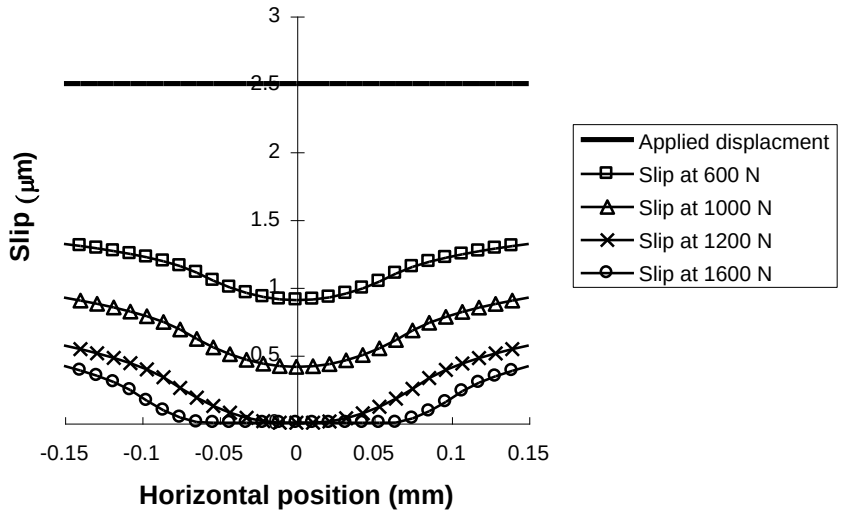

Figure 8 Comparison of slip distributions for a range of normal loads, with the same applied displacement of 2.5 μm.

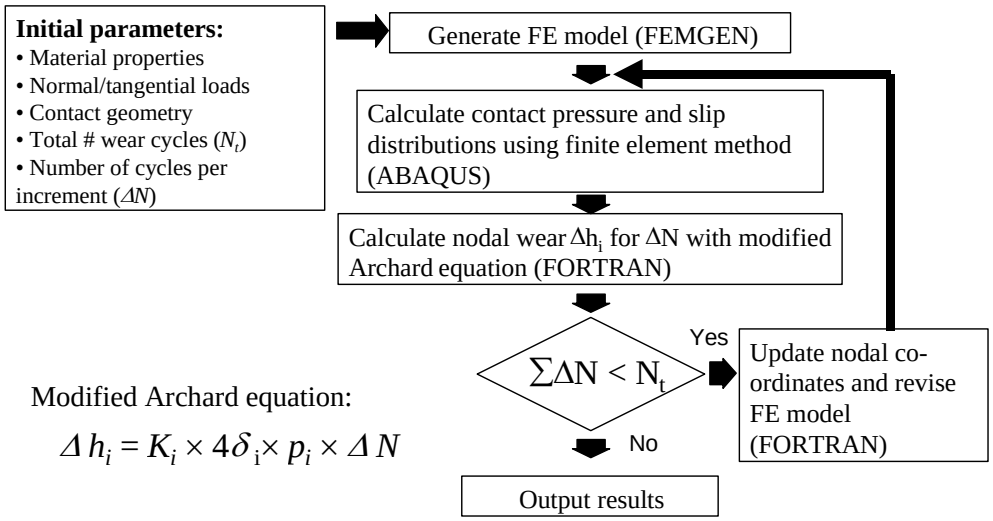

Figure 9 Flow chart of the numerical method for modelling fretting wear

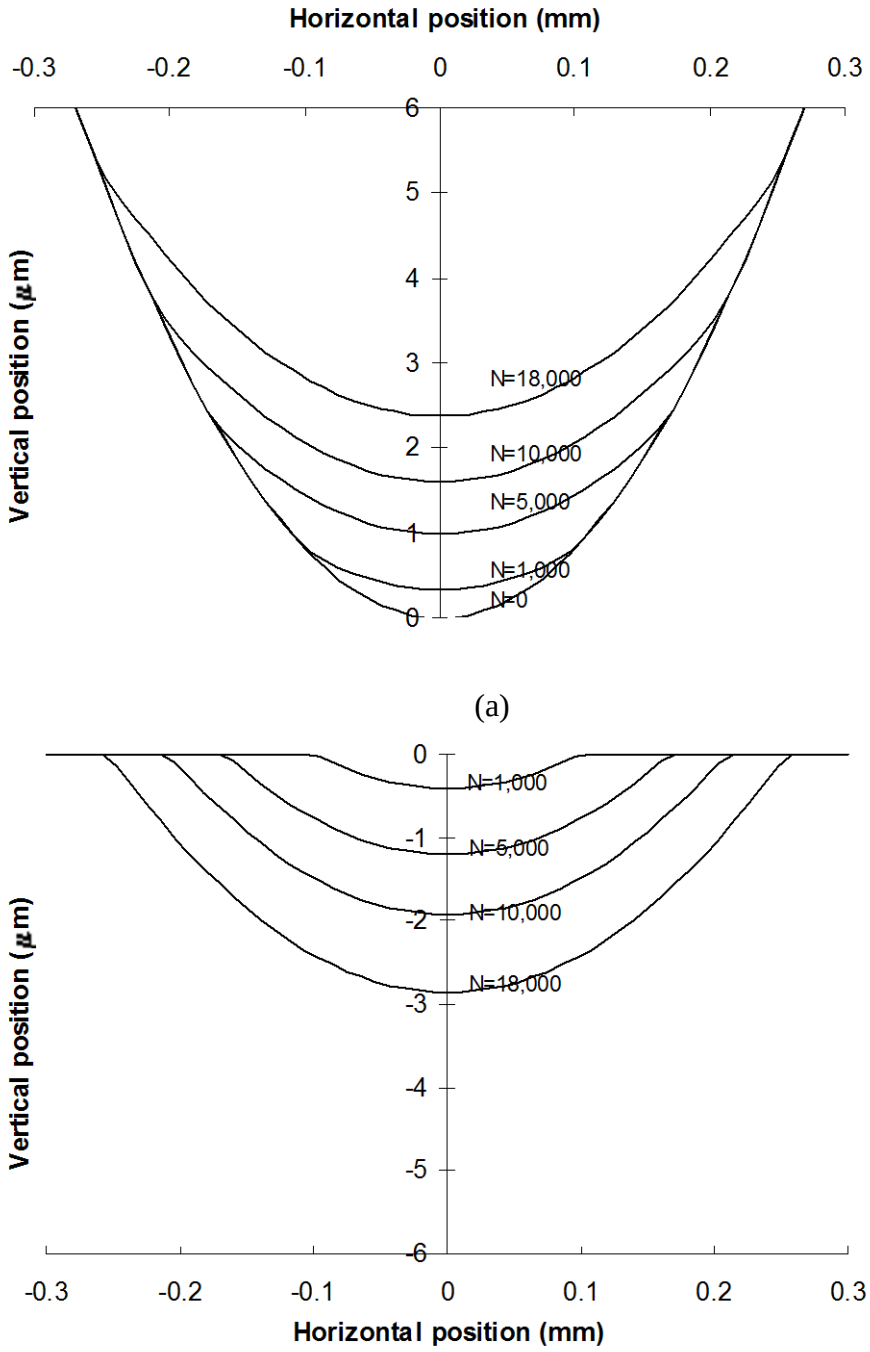

Figure 10 Predicted wear profiles for (a) cylindrical and (b) flat specimens under 185 N normal load case, for different numbers of wear cycles *N*.

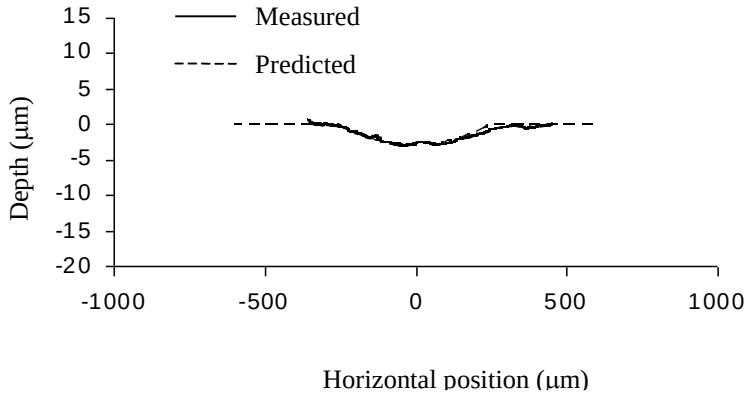

(a)

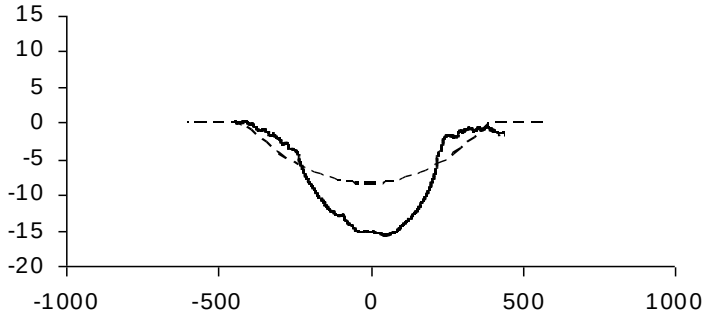

(b)

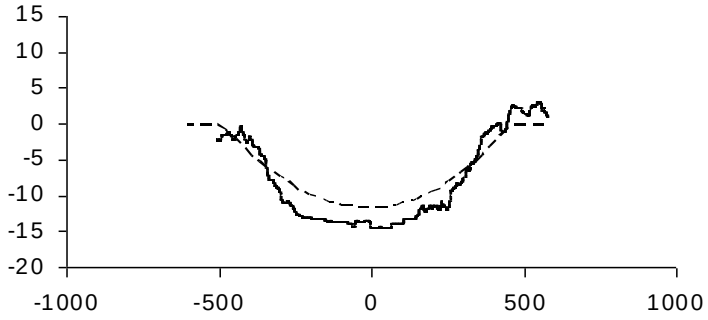

(c)

Figure 11 Comparison of FE prediction and experimental results for worn surface profiles of the flat specimen, after 18,000 wear cycle, at (a) 185N normal load, (b) 500N normal load and (c) 1670N normal load. Stroke is 50μm.

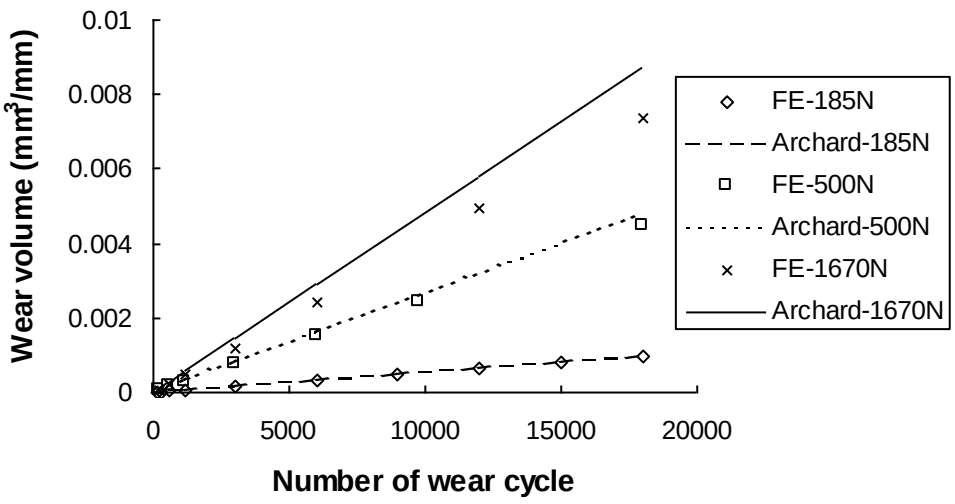

Figure 12 Comparisons of predicted wear volumes and Archard's solutions under different normal loads.

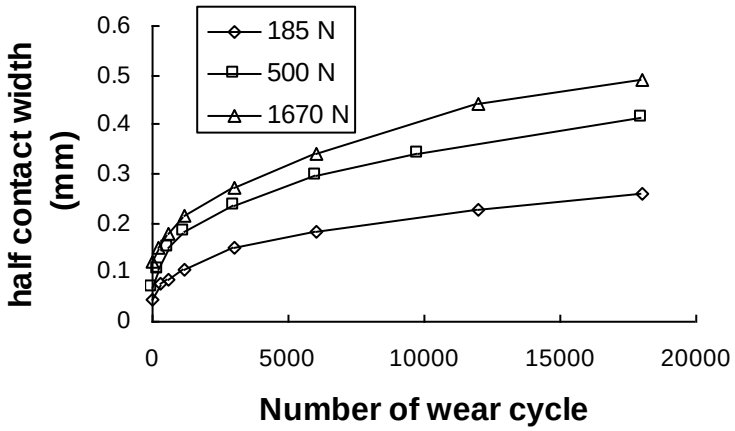

Figure 13 Evolutions of half contact widths with increasing number of wear cycles, *N*, for the different normal loads.

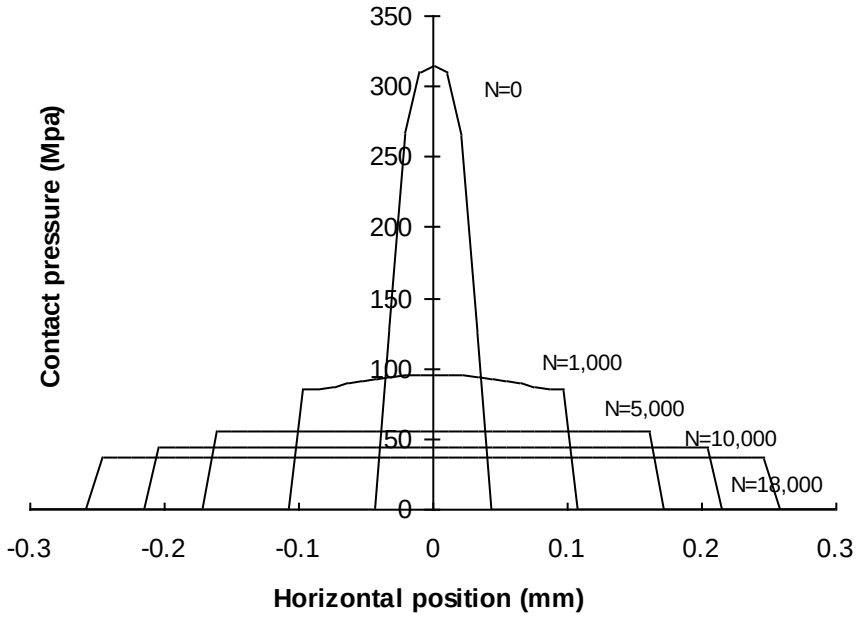

Figure 14 Predicted evolution of contact pressure with increasing number of wear cycles, *N*, under 185 N normal load case.

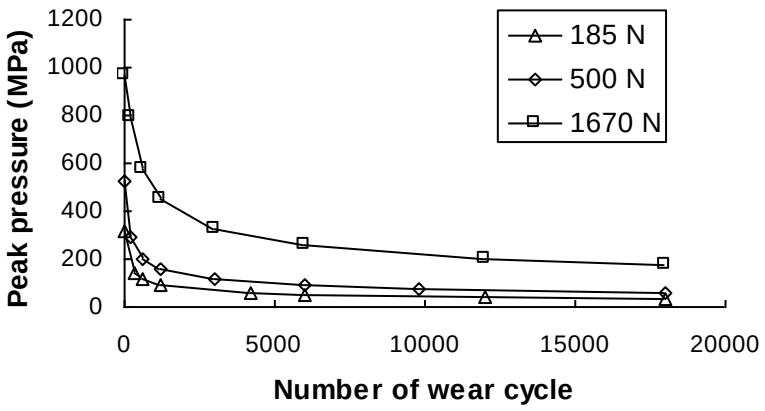

Figure 15 Evolutions of peak pressures with increasing number of wear cycles, *N*, for the different normal loads.

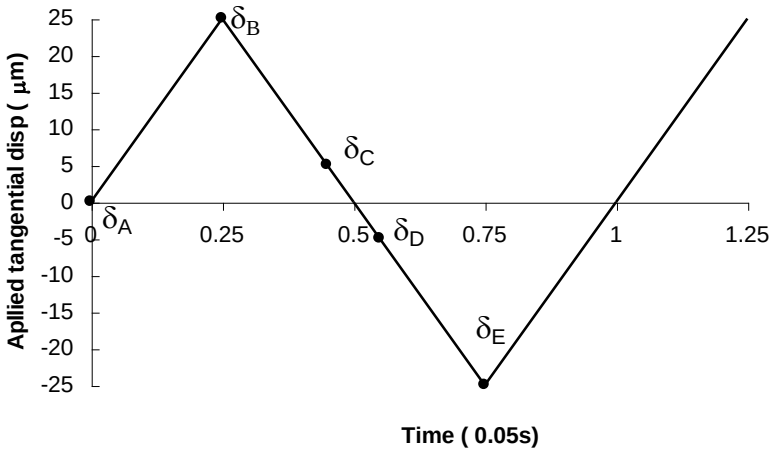

(a)

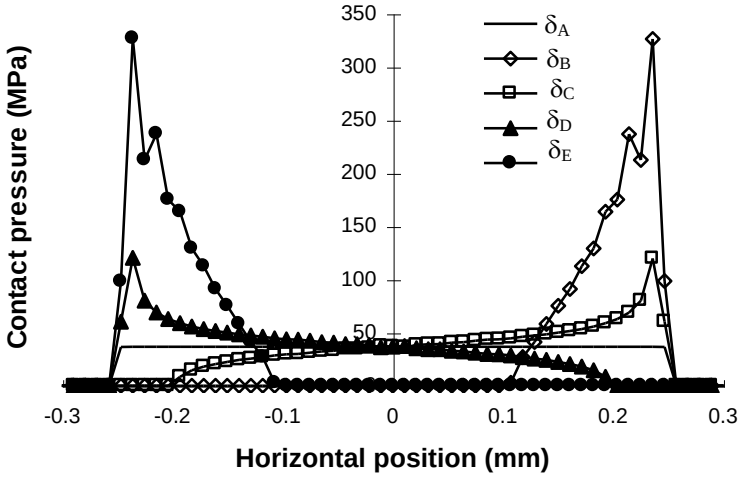

(b)

Figure 16 (a) variation of the applied tangential displacement with time and (b)variation of contact pressure with the applied tangential displacement, during 18,000th wear cycle under 185 N normal load case.

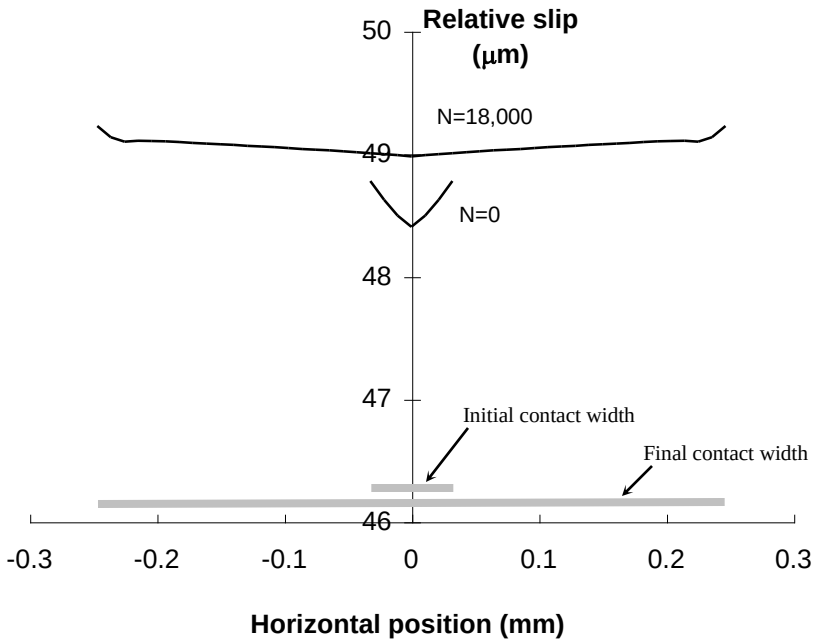

Figure 17 Predicted change of relative slip distribution due to wear damage under 185 N normal load case.

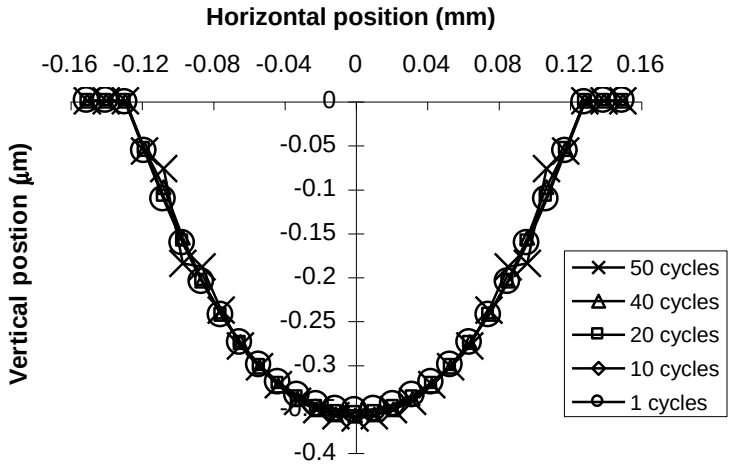

(a)

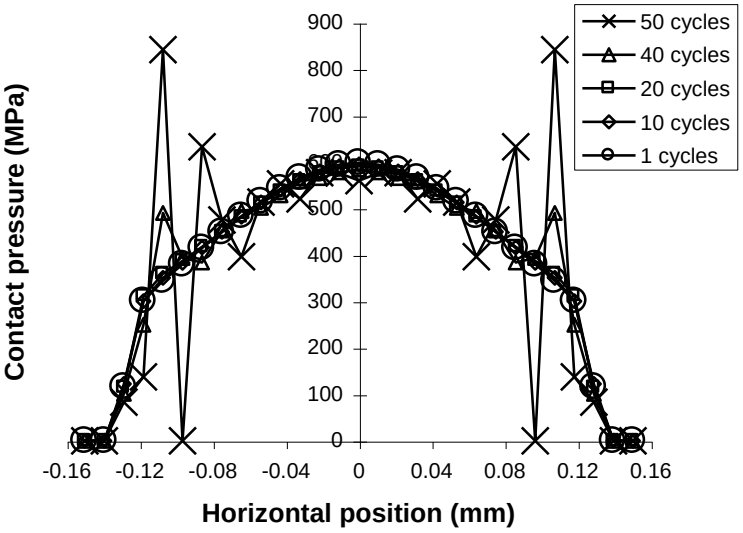

(b)

Figure 18 Effect of incremental number of fretting cycles per solution step, ΔN on (a) the worn profile of the flat specimen and (b) contact pressure. Total simulation number of cycles 200, coefficient of friction 0.6, normal load 120 N and stroke 20 μm.

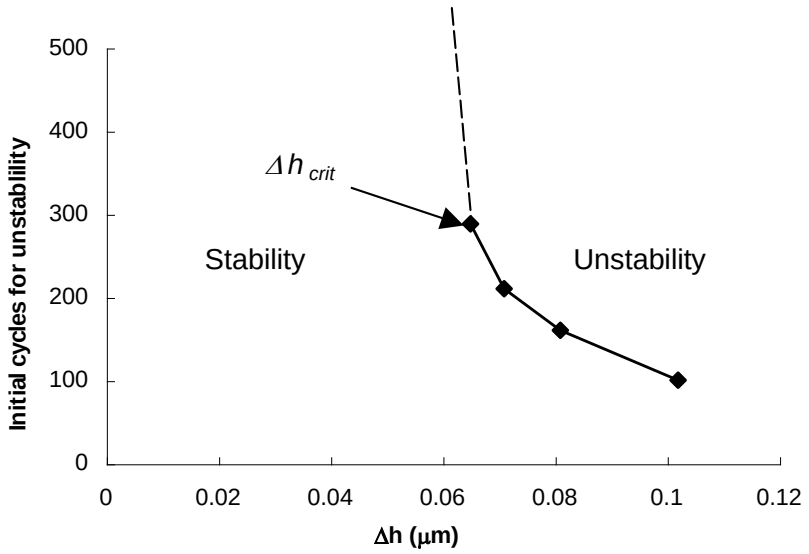

Figure 19. Influence of incremental wear depth, Δh on computational stability.

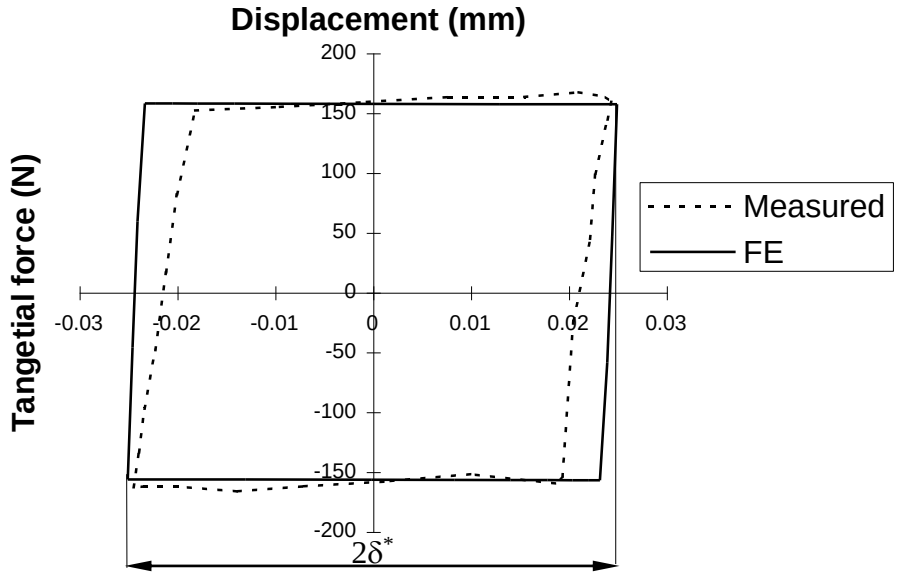

Figure 20. Comparison of the FE predicted and experimental measured tangential force versus displacement loops for 18000th wear cycle with a normal load of 185 N and an applied stroke of 50 μm.